



Microstructure prediction of multi-directional forging for 30Cr2Ni4MoV steel by the secondary development of Deform software and BP neural network

Junting Luo^{1,2} · Jingqi Zhao¹ · Zheyi Yang¹ · Yongbo Jin¹ · Chunxiang Zhang²

Received: 3 February 2021 / Accepted: 19 December 2021 / Published online: 4 January 2022
© The Author(s), under exclusive licence to Springer-Verlag London Ltd., part of Springer Nature 2022

Abstract

The true stress–strain curve of the thermal deformation of 30Cr2Ni4MoV steel was obtained by conducting a hot compression experiment. On the basis of the results, the constitutive equation of the material's thermal deformation was constructed. Then, the microstructure of the hot compression specimen was observed and analyzed, and the microstructure evolution model of 30Cr2Ni4MoV steel during thermal deformation was established accordingly. The programming of the related mathematical model was realized using the secondary development interface provided by Deform. The experimental plan was subsequently developed using an orthogonal method, and the microstructure evolution of 30Cr2Ni4MoV steel during multi-directional forging deformation was simulated. Through an orthogonal experiment analysis, the influence weight difference of each influencing factor was obtained. A back propagation neural network prediction model for the microstructure of 30Cr2Ni4MoV steel under multi-directional forging deformation was then established. The neural network prediction of the microstructure evolution of 30Cr2Ni4MoV steel under multi-directional forging was finally realized.

Keywords Multi-directional forging · Dynamic recrystallization · Orthogonal experiment · Secondary development of Deform · Back propagation neural network

1 Introduction

30Cr2Ni4MoV steel exhibits good hardenability, superior and balanced strength, high toughness and wear resistance, and good hot workability. It is often used in low-pressure rotors in large nuclear power plants [1–3]. However, this material is intrinsically coarse-grained steel, and its strong grain inheritance can easily lead to coarse grains and reduce mechanical properties [4, 5]. In recent years, the multi-directional forging process has developed rapidly. This process promotes the recrystallization of materials by applying multi-directional deformation to forging. This application helps achieve a strong grain refinement effect and greatly

improves the mechanical properties of materials. The process has low requirements for production equipment and cost. It has become an important approach to the production and performance optimization of large-scale forgings [6–9].

The plastic deformation of materials at high temperatures is a process involving multiple factors. In traditional production, the formulation of production plans and the control of the deformation process must be carried out in accordance with the results of trial production or experience. However, this requirement consumes considerable amounts of manpower and material resources. With the rapid development of computer technology, simulation has been inevitably introduced into traditional materials research [10–12]. With the aid of simulation technology, the mechanical behavior and microstructure evolution behavior of materials during and after deformation can be predicted so as to provide a reference for the formulation and optimization of production plans. By using simulation software, Qian and Pan [13] established a three-dimensional macro–micro coupled finite element model for the forging and rolling of a large AISI 4140 steel ring blank. Previous studies only focused on the

✉ Junting Luo
luojunting@ysu.edu.cn

¹ Education Ministry Key Laboratory of Advanced Forging & Stamping Technology and Science, Yanshan University, Qinhuangdao 066004, China

² State Key Laboratory of Metastable Materials Science and Technology, Yanshan University, Qinhuangdao 066004, Hebei, China

Table 1 Chemical composition of experimental material

Composition	C	Cr	Mo	Ti	Ni	Mn	Si	P	S	V	Fe
Mass fraction (%)	0.24	1.57	0.39	1.04	3.47	0.26	0.05	0.006	0.0125	0.088	18.41

geometry and thermodynamics of the ring blank. On this basis, they achieved the prediction of the evolution and distribution of the microstructure of the blank during the deformation process, which provided a reliable platform and guidance for the study of deformation mechanism and optimization of the process. To optimize the hot forging of 316LN stainless steel pipes, He et al. [14] used a modified Arrhenius-type constitutive model and an artificial neural network model in their study of the flow stress of the thermal deformation of a material. Under the condition in which both models have high reliability, the neural network has a wider prediction range than the constitutive model and is thus convenient to use with finite element analysis software.

At present, the simulation studies on the multi-directional forging process of 30Cr2Ni4MoV steel are few and thus out of proportion to the current demand for this type of material. Therefore, the current study uses the finite element simulation software called Deform to simulate the isothermal multi-directional forging of 30Cr2Ni4MoV steel, and the corresponding back propagation (BP) neural network prediction model is established. The prediction results of the two methods are then compared. The results are expected to facilitate the high-precision prediction of the multi-directional forging microstructure of 30Cr2Ni4MoV steel and guide actual production processes.

2 Hot compression experiment

2.1 Experimental material and scheme

The research object of this experiment is a type of 30Cr2Ni4MoV steel, which has been annealed after forging. Table 1 shows its main chemical composition, and Fig. 1 shows its microstructure. The structure in this state is mainly equiaxed grain, with an average grain size of about 200 μm .

The hot compression experiment is carried out on a Gleeble 3800 thermal simulator. The sample used is cylindrically shaped and measured $\phi 8 \times 12$ mm. The selected deformation temperatures are 900 $^{\circ}\text{C}$, 1000 $^{\circ}\text{C}$, 1100 $^{\circ}\text{C}$, and 1200 $^{\circ}\text{C}$; and the hot compression strain rates are 0.001, 0.01, and 0.1 s^{-1} , respectively. In an actual operation, the heating rate is 20 $^{\circ}\text{C}$ per second, and the sample is heated to a predetermined temperature and then kept

warm. The compression rate of deformation is 70%. After compression, the sample is immediately cooled to retain the deformed structure.

2.2 Experimental results

The true stress–strain curve of the thermal deformation of the material is established on the basis of the experimental data of hot compression. Figure 2 shows the comparison between the curves of different strain rates at the same deformation temperature. Observation and analysis reveal that these curves present obvious three-stage changes. At the initial stage of deformation, the stress increases sharply due to work hardening. However, this increasing trend gradually slows down due to the subsequent dynamic recovery. The stress begins to decrease after reaching the peak value because the softening ability of dynamic recrystallization and recovery exceeds the effect of work hardening. At the end of the deformation, the stress tends to be stable, thereby reflecting the dynamic balance of softening and work hardening. The peak stress statistics under various deformation conditions are shown in Table 2. The joint analysis of the data in Table 2 and the curve in Fig. 2 shows that the strain rate is proportional to the peak stress and that the deformation temperature is inversely proportional to the peak stress. These data serve as the basis for the construction of the constitutive equation of the thermal deformation of 30Cr2Ni4MoV steel.

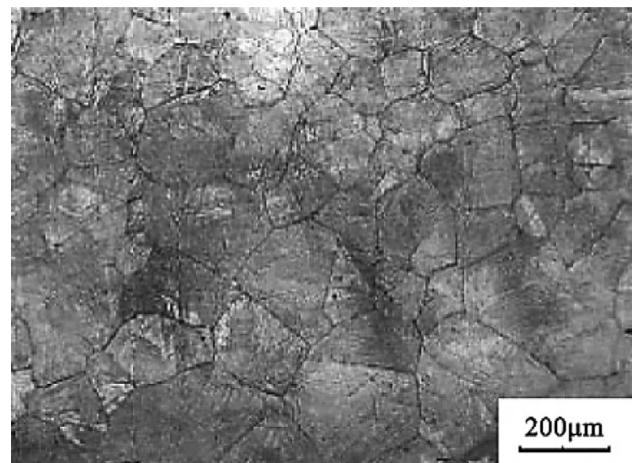


Fig. 1 Microstructure of experimental material

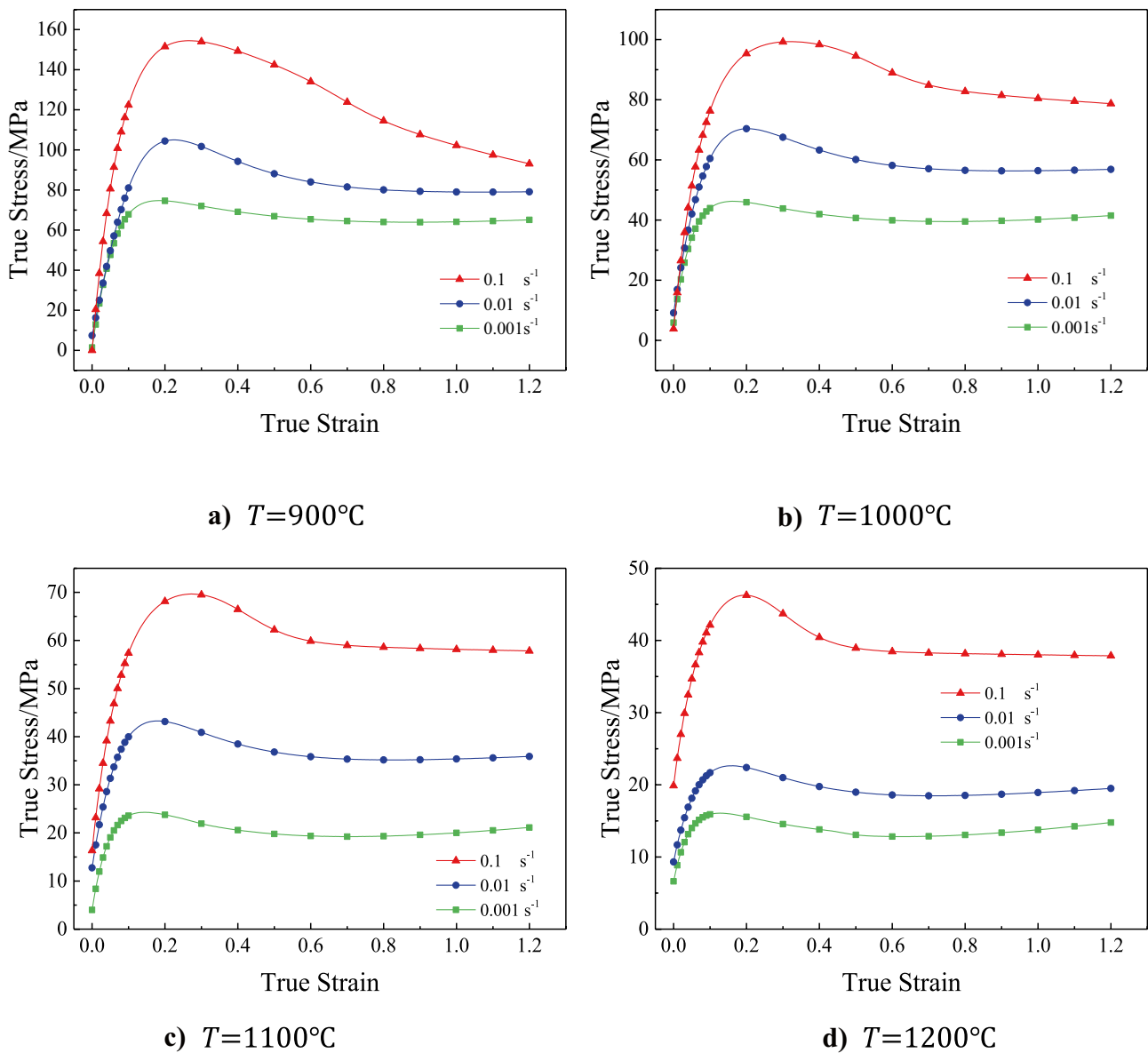


Fig. 2 True stress–strain curves at different strain rates. **a)** $T = 900\text{ }^{\circ}\text{C}$. **b)** $T = 1000\text{ }^{\circ}\text{C}$. **c)** $T = 1100\text{ }^{\circ}\text{C}$. **d)** $T = 1200\text{ }^{\circ}\text{C}$

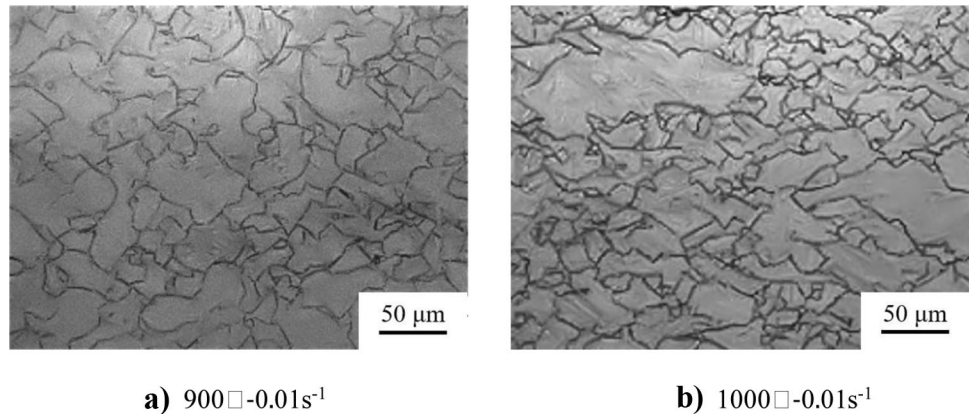
The change state of the true stress–strain curve shows that 30Cr2Ni4MoV steel undergoes obvious dynamic recrystallization during thermal deformation. Figure 3

shows the microstructure of samples under deformation conditions of $900\text{ }^{\circ}\text{C}$ – 0.01 s^{-1} and $1000\text{ }^{\circ}\text{C}$ – 0.01 s^{-1} in the hot compression experiment. It can be seen that the microstructure has obvious dynamic recrystallization characteristics. The metallographic microstructure of samples under different hot compression deformation conditions is observed and analyzed, and the dynamic recrystallization volume fraction (X_{drex}) is obtained by calculating the proportion of area, and the dynamic recrystallization grain size (D_{drex}) is measured by using the transection method. The above data are counted in Table 3, which will be used as the basis for establishing the microstructure evolution model.

Table 2 Peak stress under various deformation conditions

Peak stress/MPa		Deformation temperature/ $^{\circ}\text{C}$			
		900	1000	1100	1200
Strain rate/ s^{-1}	0.001	74.68	46.23	24.27	16.06
	0.01	104.95	70.37	43.26	22.63
	0.1	154.45	99.32	69.64	46.26

Fig. 3 Microstructure of hot compression sample. a) 900 °C–0.01 s⁻¹. b) 1000 °C–0.01 s⁻¹



3 Deform simulation of multi-directional forging of 30Cr2Ni4MoV steel

3.1 Related mathematical models and secondary development of Deform

The constitutive equation of the thermal deformation of materials and various microstructure evolution models are important foundations for the finite element simulation of the plastic deformation process. Based on the true stress–strain curve obtained from the experiment, the constitutive equation of the material is constructed in the form of a hyperbolic sinusoidal function in the Arrhenius model [15, 16]. Based on the statistics and analysis of the hot compression microstructure, various thermal deformation microstructure evolution models of the material are constructed by using the Sellers model and Avrami dynamic recrystallization theory [17, 18].

The constitutive equation of the thermal deformation of 30Cr2Ni4MoV steel is as follows:

$$\dot{\varepsilon} = 3.34 \times 10^{11} \times [\sinh(0.018\sigma_p)]^{3.6} \times \exp\left(-\frac{347,000}{RT}\right) \quad (1)$$

$\dot{\varepsilon}$ is the strain rate, σ_p is the peak stress, R is the gas constant (8.314 J/(mol K)⁻¹), and T is the deformation temperature.

The microstructure evolution model of the thermal deformation of 30Cr2Ni4MoV steel is shown below. The model includes the expression of the dynamic recrystallization critical condition, dynamic recrystallization volume fraction, and dynamic recrystallization grain size.

$$\begin{cases} \varepsilon_p = 0.008Z^{0.11} \\ \varepsilon_c = (0.6 \sim 0.85)\varepsilon_p \\ X_{drex} = 1 - \exp\left[-1.08\left(\frac{\varepsilon - \varepsilon_c}{\varepsilon_p}\right)^{1.89}\right] \\ D_{drex} = 5.9 \times 10^4 Z^{-0.243} \end{cases} \quad (2)$$

X_{drex} is the dynamic recrystallization volume fraction, D_{drex} is the dynamic recrystallization grain size, ε_p is the peak strain, ε is the strain, ε_c is the critical strain, and Z is the compensation factor of the deformation temperature to the strain rate obtained by the following formula:

$$Z = \dot{\varepsilon} \exp\left(\frac{347,000}{RT}\right) \quad (3)$$

The average grain size of the structure after dynamic recrystallization is called the average grain size of dynamic recrystallization (D_{avg}), which is calculated according to the following formula:

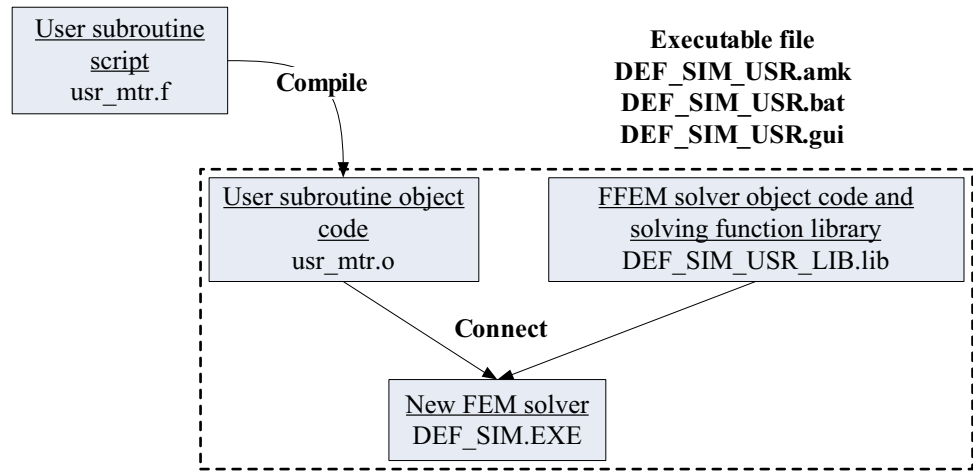
$$D_{avg} = D_{drex}X_{drex} + D_0(1 - X_{drex}) \quad (4)$$

The Deform software provides two secondary development methods, namely pre-processing and post-processing secondary development. In this work, the custom subroutine is compiled in the pre-processing stage, and the constitutive equation of the thermal deformation of 30Cr2Ni4MoV steel

Table 3 Statistics related to dynamic recrystallization

Strain rate/s ⁻¹	Deformation temperature/°C	$X_{drex}/\%$	$D_{drex}/\mu\text{m}$
0.001	900	97.0	40
	1000	99.9	72
	1100	100.0	132
	1200	99.9	224
0.01	900	81.0	54
	1000	98.5	43
	1100	99.9	76
	1200	100.0	128
0.1	900	49.0	108
	1000	87.0	46
	1100	99.0	45
	1200	99.9	73

Fig. 4 Schematic of pre-processing secondary development



is written into the flow stress script (USRMTR). Figure 4 presents the schematic of the pre-processing secondary development. In the post-processing stage, the microstructure evolution model, including the dynamic recrystallization critical conditions, dynamic recrystallization volume fraction, and dynamic recrystallization grain size, is compiled into the script file (pstusr.f) and linked to the dynamic link library file (USR_DEF_PST3.dll). The display of custom variables is realized by calling the library on the post-processing interface. Figure 5 shows the schematic of the post-processing secondary development.

3.2 Establishment of finite element model

The multi-directional forging process mainly includes multi-directional free forging, multi-directional die forging, and multi-directional extrusion. Their basic principle is to apply multi-directional plastic deformation to a blank to promote the dynamic recrystallization of the material, and refine the microstructure, and improve the macroscopic strength [19–21]. In this work, the isothermal multi-directional die

forging of 30Cr2Ni4MoV steel is studied. The specific processes include closed multi-directional forging (CMDf), bilateral open multi-directional forging (BOMDF), and single-side open multi-directional forging (SSOMDF). First, the geometric model corresponding to each process is established. Four-node tetrahedral elements are selected to divide a blank into 25,000 tetrahedral element meshes. Shear friction is selected as the friction property, and the friction factor is set to 0.3. The final constructed finite element model is shown in Fig. 6. In the post-processing of the simulation results, the user-defined variables are extracted according to the intercepting plane method shown in Fig. 6d.

The mold structures of the three multi-directional forging processes show differences. The initial position of the blank of the first two processes is the geometric center of the mold cavity. By contrast, the blank of the SSOMDF process is placed on one side of the cavity. Thus, the stress state of the blank is not consistent during the deformation process. Each loading up to the preset deformation is defined as one pass deformation. At the end of each pass deformation, the CMDf and BOMDF blanks flip along

Fig. 5 Schematic diagram of post-processing secondary development

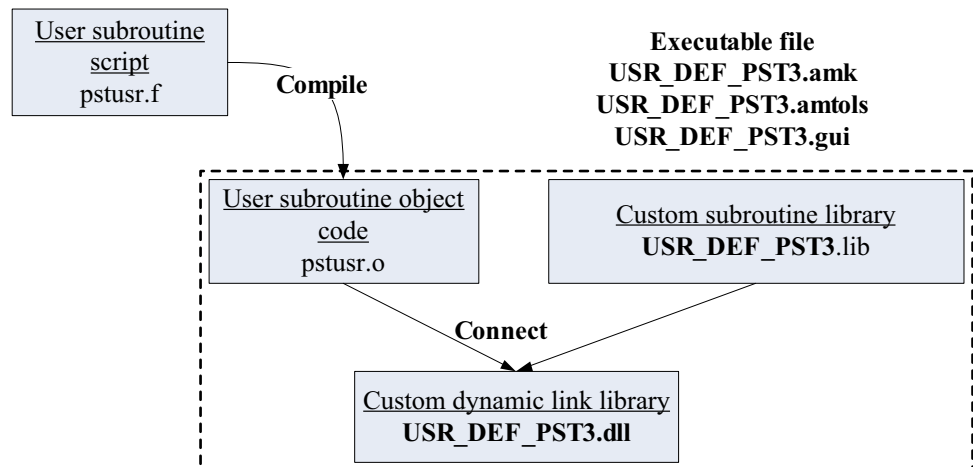
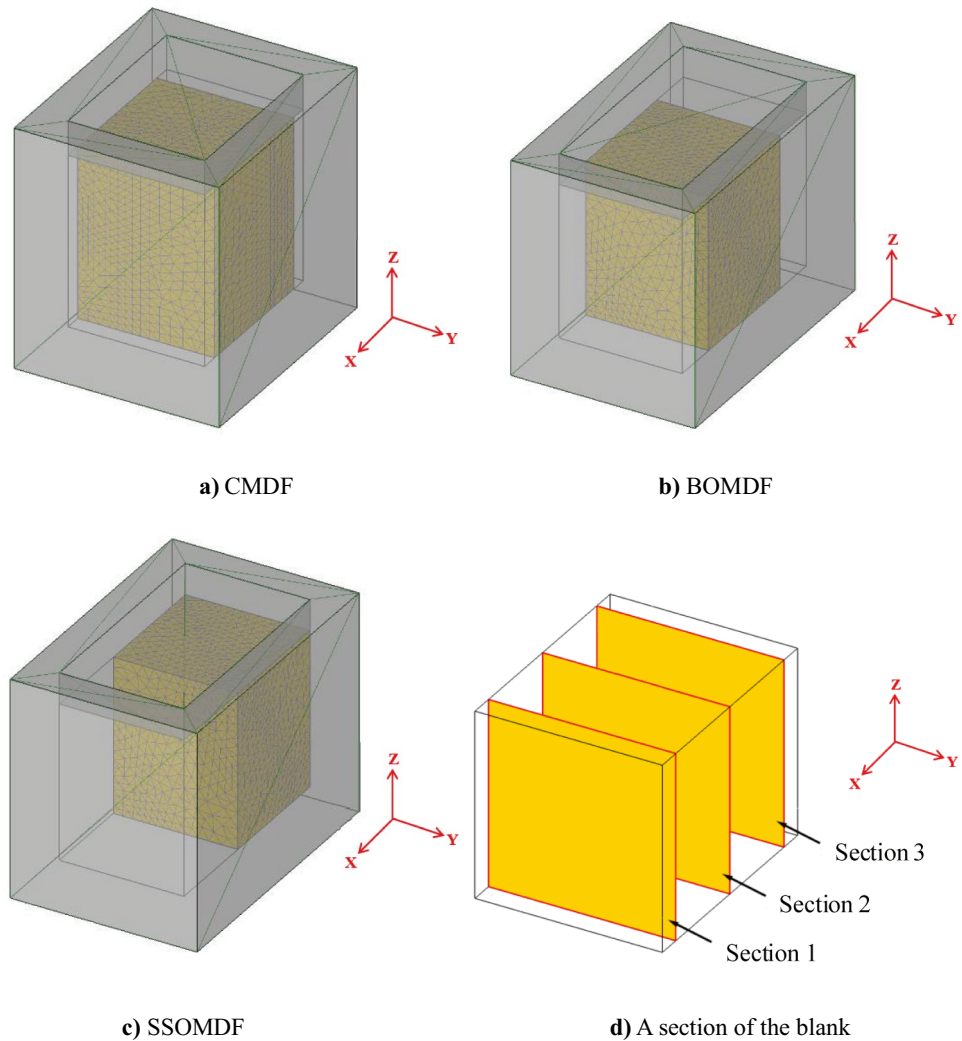


Fig. 6 Finite element model. **a)** CMDF. **b)** BOMDF. **c)** SSOMDF. **d)** A section of the blank



the X and Y directions, respectively, so that the next pass deformation in another loading direction is applied to the blank. After each pass deformation of the SSOMDF, the blank is overturned along the X, Y, and Z directions, and the cycle is carried out so as to achieve uniform deformation of the blank. Aside from the mold structure, the main impact factors of the dynamic recrystallization behavior of the material also include deformation temperature, strain rate, and single pass deformation. To reduce the time cost of the simulation, we use an L9 (3⁴) orthogonal table in

the experimental design. The final determined orthogonal table, that is, the simulated grouping, is shown in Table 4. In the table, C represents a CMDF die, B represents a BOMDF die, and S represents a SSOMDF die. The initial grain size of the material is defined as 58.9 μm, and each group of processes undergoes nine passes of deformation. Corresponding to single pass deformation of 20%, 30%, and 40%, the dimensions of the cuboid forging blanks set are 40 × 40 × 50, 35 × 35 × 50, and 30 × 30 × 50 mm, respectively.

Table 4 Orthogonal table

Level value		Process number								
		1	2	3	4	5	6	7	8	9
Impact factors	Temperature/°C	900	900	900	1100	1100	1100	1300	1300	1300
	Strain rate/s ⁻¹	0.1	1	10	0.1	1	10	0.1	1	10
	Single pass deformation/%	20	30	40	30	40	20	40	20	30
	Mold structure	C	B	S	S	C	B	B	S	C

3.3 Analysis and discussion of simulation results

Process 3, process 6, process 8, and process 9 are taken as examples to briefly summarize the microstructure simulation results of the multi-directional forging deformation of the blank.

The simulation result of process 3 is shown in Fig. 7. Among the first three groups of processes with a deformation temperature of 900 °C, the single pass deformation and strain rate of process 3 are the largest. The blank after three passes of deformation has a relatively high degree of recrystallization on the right side of the *x*-axis direction. After six passes of deformation, the blank basically reaches complete dynamic recrystallization. The minimum grain size after nine passes of deformation is as low as 1.45 μm. This group uses a SSOMDF die. After nine passes of deformation, the grain size of the core of the blank and the free surface area near the left side of the blank’s *x*-axis direction are slightly large, and the small-sized grains are mostly distributed in the surface area of the blank. However, the gap between grain sizes is small. The overall structure is uniform.

The cloud diagram of the simulation results of the blank under the condition of process 6 is shown in Fig. 8. The deformation temperature of this process is 1000 °C. The strain rate is high, but the single pass deformation is low. After three passes of deformation, the dynamic recrystallization of the blank is not complete, but after six passes, it can basically achieve complete dynamic recrystallization. However, the degree of change in the grain size of the blank after deformation from six passes to nine passes is not obvious, thus indicating a limit to grain refinement. This result

may be due to the fact that the billet obtains small-sized grains after six passes of deformation and excessive grain boundaries require a large driving force for recrystallization. At a low single pass deformation, the energy brought by the further accumulation of passes is not enough to drive recrystallization.

The simulation result of process 8 is shown in Fig. 9. The deformation temperature of this group is 1300 °C, and the simulation result shows that the degree of grain size refinement of this group is extremely small. This result is mainly due to the deformation temperature of process 8 being relatively high and the strain rate being adequately low. The crystal grains first absorb energy and expand. Then, dynamic recrystallization occurs with the accumulation of deformation.

The simulation result of process 9 is shown in Fig. 10. The strain rate under this group of processes is increased to 10 s⁻¹, and the single pass deformation is 30%. The simulated cloud image shows that the influence of a high temperature under this process is lower than that of a high strain rate. The blank is completely recrystallized after three passes of deformation, and the overall average grain size is refined to about 20 μm after nine passes of deformation.

The blank can be completely recrystallized under each set of process conditions. Hence, this section does not discuss the relationship between deformation conditions and volume fraction. Table 5 shows the average grain size of the blank after deformation under each set of process conditions. To quantitatively analyze the impact of each factor, we take the average grain size of the blanks deformed in three, six, and nine passes under each group of processes as the research index. The average value and

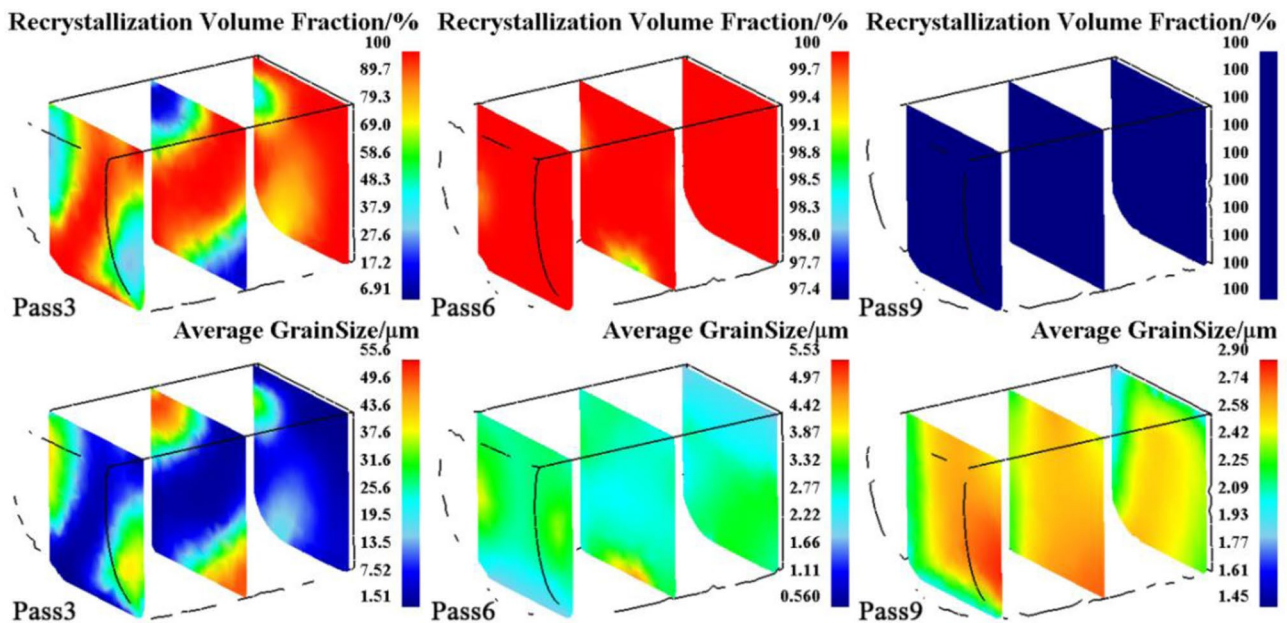


Fig. 7 Simulation results of process 3

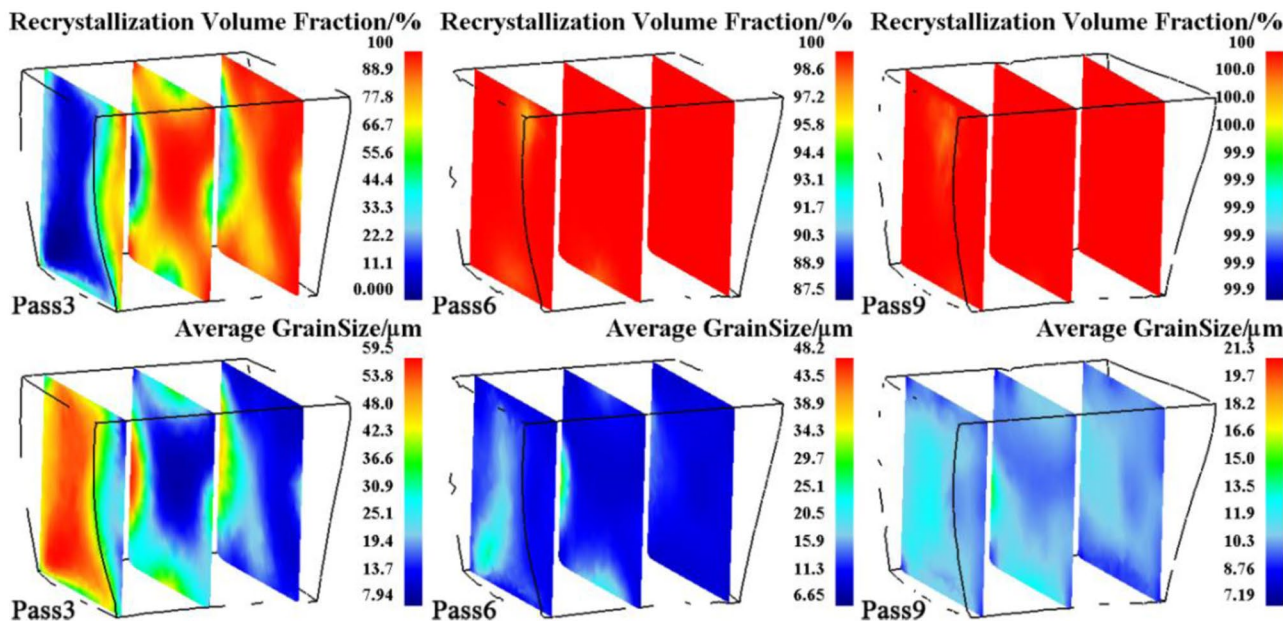


Fig. 8 Simulation results of process 6

range of the index corresponding to the value of each factor are then calculated. The results are shown in Table 6.

According to the range calculation results in Table 6, the range value of temperature is the largest for the average grain size after deformation regardless of the number of passes. This result shows that the factor exerts a major effect on the average grain size of the blank. The range of strain rate is the second, which indicates the factor's strong role. The range of the mold structure ranks third while the range of single pass deformation ranks fourth; hence, the influence of these two factors is weakened in turn. The average value of the index corresponding to

the different values of each factor shows that as the deformation temperature increases, the average grain size of the blank after multi-directional forging also increases. When the strain rate is increased, the blank can obtain a fine average grain size. In this simulation, the change in the deformation value of a single pass does not reflect a linear effect. For the three deformations in this study, the grain size of the blank is slightly low when the value is 30%. According to the simulation examples, the differences in the mold structure directly affect the deformation behavior of the blank and further influence the distribution of recrystallization and structure. According to the average values shown

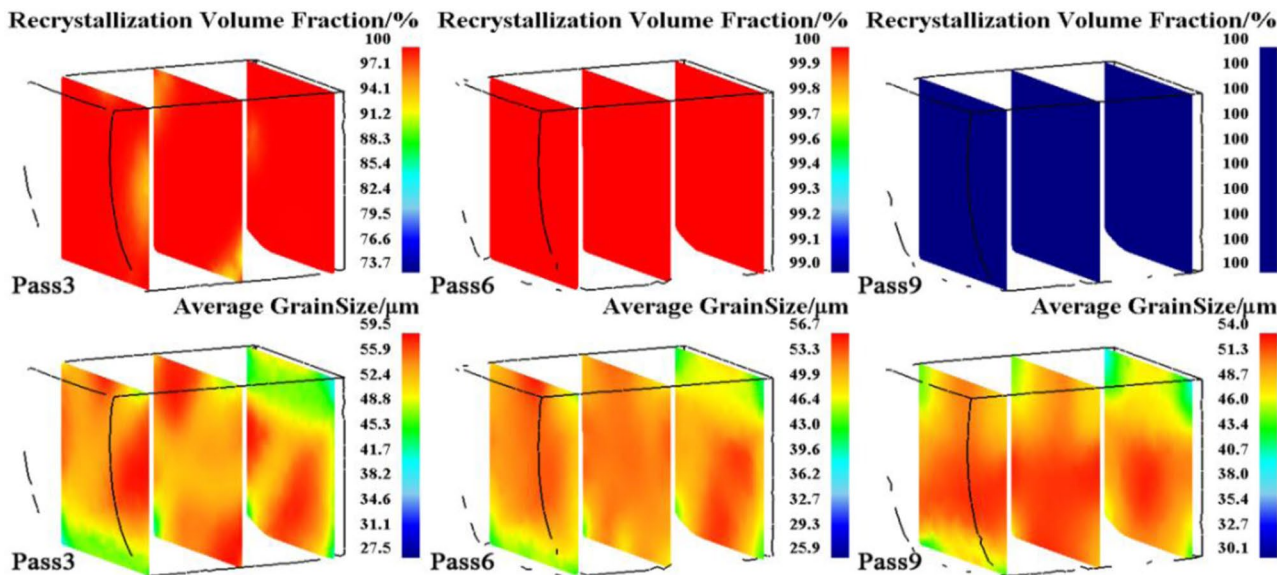


Fig. 9 Simulation results of process 8

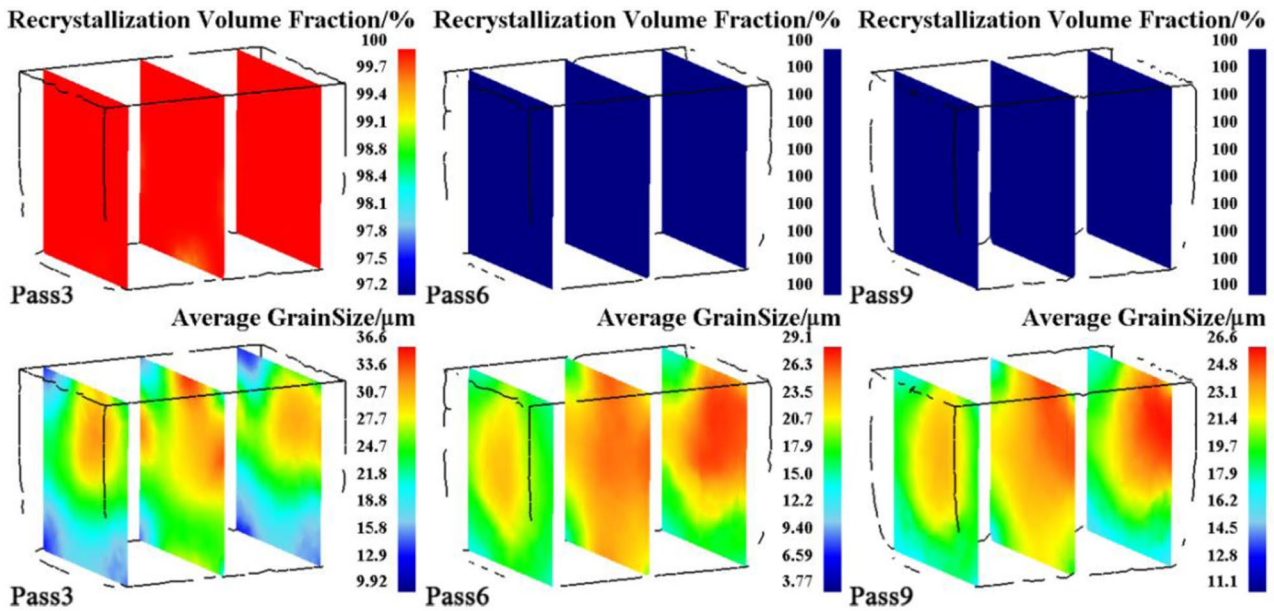


Fig. 10 Simulation results of process 9

in Table 6, the use of CMDF die can obtain a fine structure, and the SSOMDF die and BOMDF die have similar grain sizes and high values. In terms of the values involved in the various influence factors in this study, the deformation temperature can be set to below 1100 °C, the strain rate can be set to above 1 s⁻¹, and the single pass deformation can be set to 30% to obtain a fine and uniform multi-directional forging structure. Furthermore, a CMDF die may be used. According to the data in Tables 5 and 6, except for individual conditions, the average grain size of the blank decreases with an increase in the number of multi-directional forging passes. Therefore, the processing pass can be set to nine passes.

4 Prediction of multi-directional forging microstructure of 30Cr2Ni4MoV steel based on BP neural network

The accuracy of finite element simulation is greatly affected by the accuracy of related mathematical models. Simulations based on fixed-form models cannot easily achieve a comprehensive expression of complex macro- and microevolution laws during the thermal deformation of materials. The original intention of artificial neural network technology is to imitate the

human brain’s information processing method, which is suitable for solving various types of complex nonlinear relationships. The BP neural network technology is widely used and can achieve an accurate approximation of arbitrary nonlinear relationships [22, 23]. Therefore, this work further uses a BP neural network to predict the microstructure of the blank deformed under different multi-directional forging process conditions.

4.1 Neural network modeling

A typical BP neural network includes three network layers: input layer, hidden layer, and output layer. The content of the input layer and output layer needs to be determined according to the finite element simulation results. The deformation process of the material involves a variety of influencing factors. The analysis of the orthogonal experiment results indicates that the roles of each factor and the influence weight are quite different. Hence, this study establishes different neural network models. In one neural network model that directly affects the dynamic recrystallization behavior, deformation temperature, strain rate, and true strain are used as the input layer. For the output layer, dynamic recrystallization volume fraction and average grain size are used. In another neural network model

Table 5 Average grain size statistics

Average grain size value/μm	Process number								
	1	2	3	4	5	6	7	8	9
Pass 3	25.0	19.6	16.0	34.0	14.0	30.2	59.7	52.8	23.1
Pass 6	8.64	6.08	2.96	31.7	13.0	13.5	58.7	50.6	20.6
Pass 9	7.09	4.94	2.45	28.5	12.5	11.1	59.0	49.5	20.0

Table 6 Processing of orthogonal experiment results

Number of passes	Project	Temperature (°C)	Strain rate (s ⁻¹)	Single pass deformation (%)	Mold structure				
Pass3	Average value	900	20.2	0.1	39.6	20	36	C	20.7
		1100	26	1	28.8	30	25.6	B	36.5
		1300	45.2	10	23.1	40	29.9	S	34.3
	Range	25	16.5	10.4	15.8				
Pass6	Average value	900	5.9	0.1	33.0	20	24.2	C	14.1
		1100	19.4	1	23.2	30	19.5	B	26.1
		1300	43.3	10	12.4	40	24.9	S	28.4
	Range	37.4	20.6	5.4	14.3				
Pass9	Average value	900	4.8	0.1	31.5	20	22.6	C	13.2
		1100	17.4	1	22.3	30	17.8	B	25
		1300	42.8	10	11.2	40	24.7	S	26.8
	Range	38	20.3	6.9	13.6				

that directly affects the strain distribution, the number of deformation passes, mold structure, and single pass deformation are used as the input layer. For the output layer, true strain is used. The range of the number of neurons in the hidden layer of the former is set to 3–12, and that of the latter is set to be 2–12. The selection of this value depends on the following formula:

$$num = \sqrt{m + n} + a \quad (0 \leq a \leq 10) \tag{5}$$

num represents the number of neurons in the hidden layer, *m* is the number of nodes in the input layer, and *n* is the number of nodes in the output layer.

In the BP neural network system, the size of the weight is proportional to the strength of the connection between neurons, and the node transfer function is the medium for neuron weight transfer. Therefore, choosing the appropriate node transfer function is important to ensure the fitting accuracy of the neural network. In this study, the sigmoid function is used in the hidden layer while the linear function is used in the output layer. Given a different number of neuron nodes, the function fit is achieved.

A definite neural network topology architecture is established accordingly (Fig. 11).

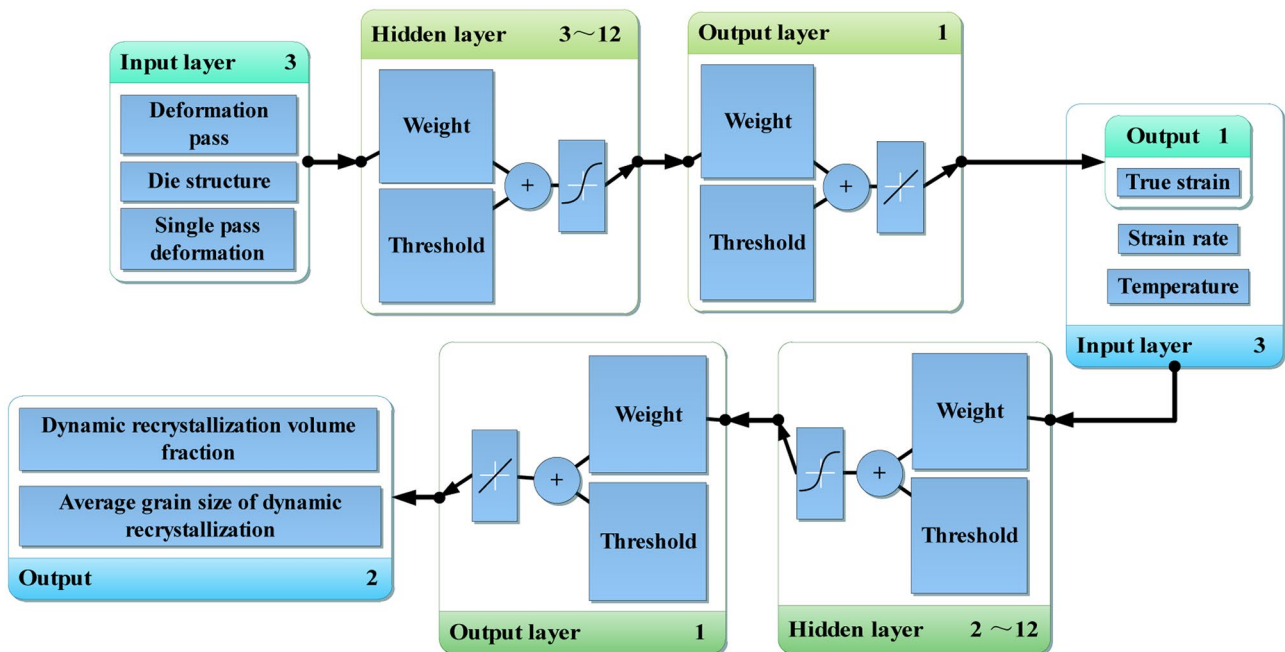


Fig. 11 Neural network topology architecture

Table 7 Experimental conditions

Group	Strain rate/s ⁻¹	Temperature/°C	Mold structure	Reduction	Deformation pass
1	1	900	S	0.1	9
2	0.01	1050	B	0.2	6
3	0.1	1100	C	0.3	3

4.2 Neural network prediction results and discussion

Based on the data obtained from the hot compression experiment, the established neural network model is trained and adjusted repeatedly, and finally the network model with good regression effect and strong generalization ability is obtained. This study uses the GUI development function provided by MATLAB to compile the neural network model into an executable function. The relevant deformation parameters are entered into the front-end interface, and the corresponding neural network prediction results are then obtained. This study randomly

selects three groups of experimental conditions (Table 7) and carries out the neural network prediction of the multi-directional forging deformation of 30Cr2Ni4MoV steel. The dynamic recrystallization volume fraction and average grain size prediction data of the blank after deformation are then obtained. The method of intercepting the plane on the blank is the same as the finite element simulation above, and the prediction results of the three sections are obtained and compared with the finite element simulation results under the same experimental conditions (Figs. 12, 13 and 14).

The comparison of the prediction results under various conditions shows that the dynamic recrystallization

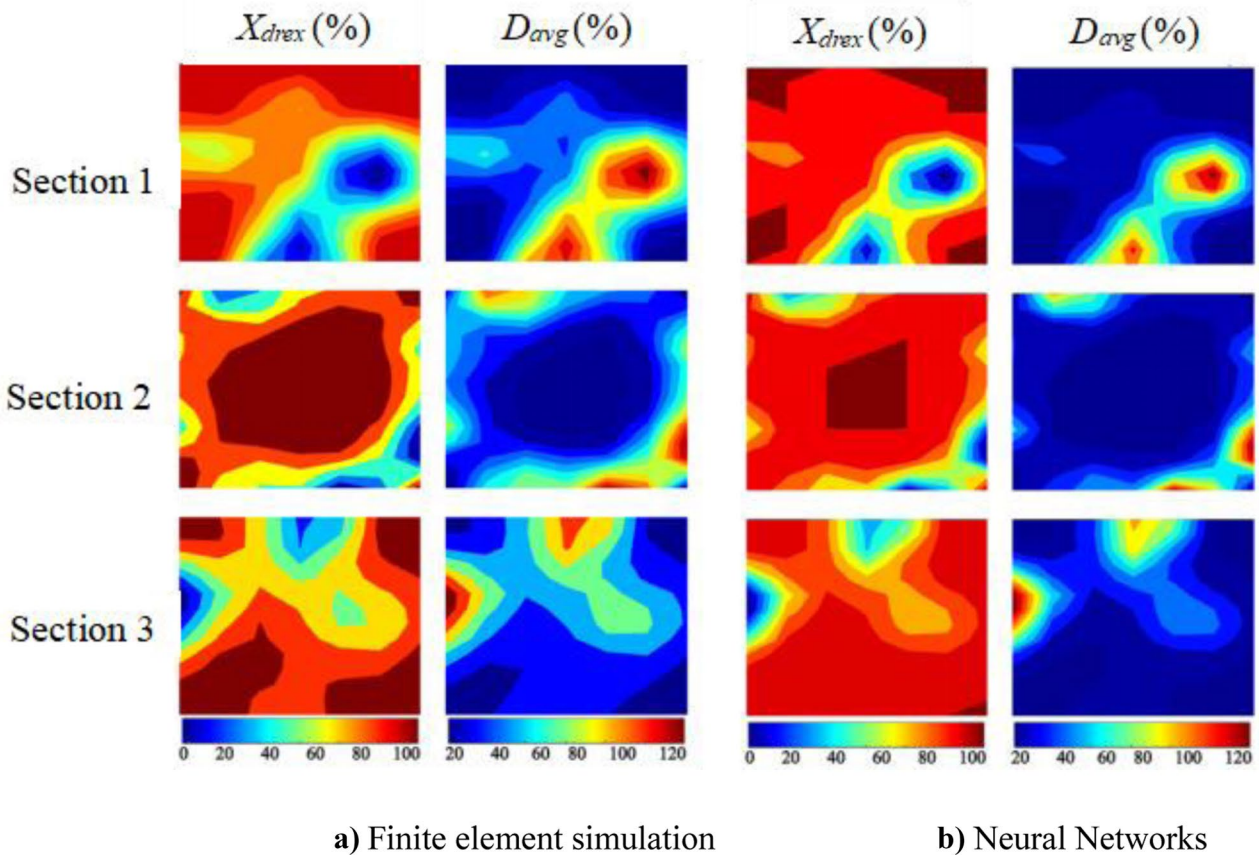


Fig. 12 Comparison of group 1. **a)** Finite element simulation. **b)** Neural networks

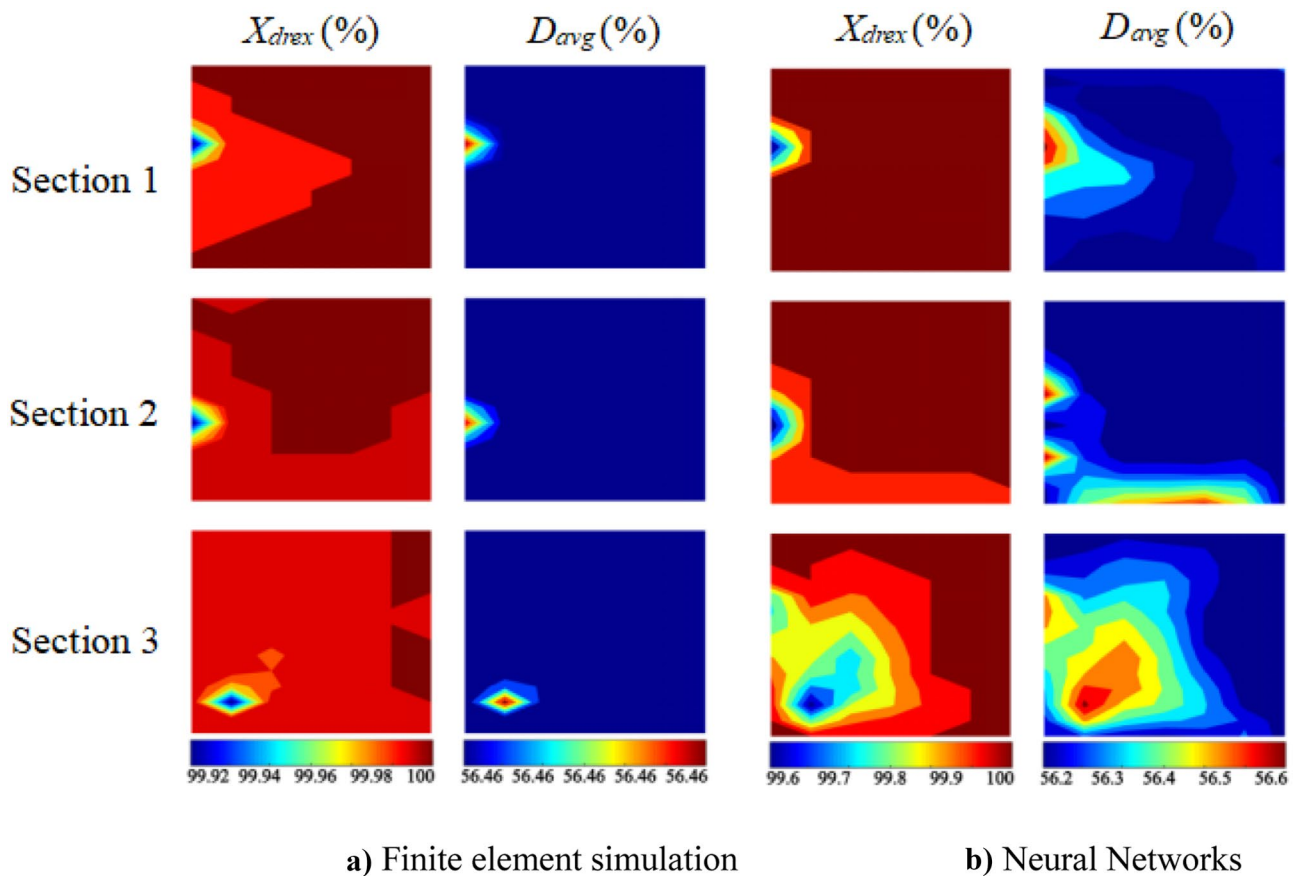


Fig. 13 Comparison of group 2. **a)** Finite element simulation. **b)** Neural networks

volume fraction and average grain size prediction results obtained by the two methods are basically the same. However, the recrystallization area and average grain size distribution of the blank predicted by the neural network are more detailed than those by the finite element simulation. Moreover, the transitional stratification changes between different recrystallization degrees and grain sizes are particularly obvious. This feature is particularly significant in the prediction results of the second and third groups of conditions shown in Figs. 13 and 14. Taking condition 2 as an example, for the dynamic recrystallization volume fraction, the finite element simulation results show that the small area on the left and the lower left corner of each slice shows multiple color layers, and most of the remaining areas are displayed as two similar red. Combined with the legend below the picture, the dynamic recrystallization volume fraction of each area of the blank is above 99.9%, and the difference between them is very small. In this state, the predicted result of the grain size distribution given by the finite

element simulation is consistent with the volume fraction distribution and gets a single grain size value. The prediction result of the neural network shows that the dynamic recrystallization volume fraction of each area of the blank is above 99.6%, which is 0.3% lower than the finite element simulation result, but the volume fraction on each slice obviously has more transitional layers and richer details. The grain size predicted by the neural network is not a single value, and the distribution state is consistent with the recrystallized volume fraction, and correspondingly shows an obvious layered change process. It is analyzed that the finite element simulation based on fixed-form of mathematical models is less flexible. The neural network with strong nonlinear relationship fitting ability showed a more detailed division of microstructure distribution in the abovementioned comparative experiment. Therefore, it is believed that the established neural network prediction model can be used to predict the microstructure of 30Cr2Ni4MoV steel in multi-directional forging deformation.

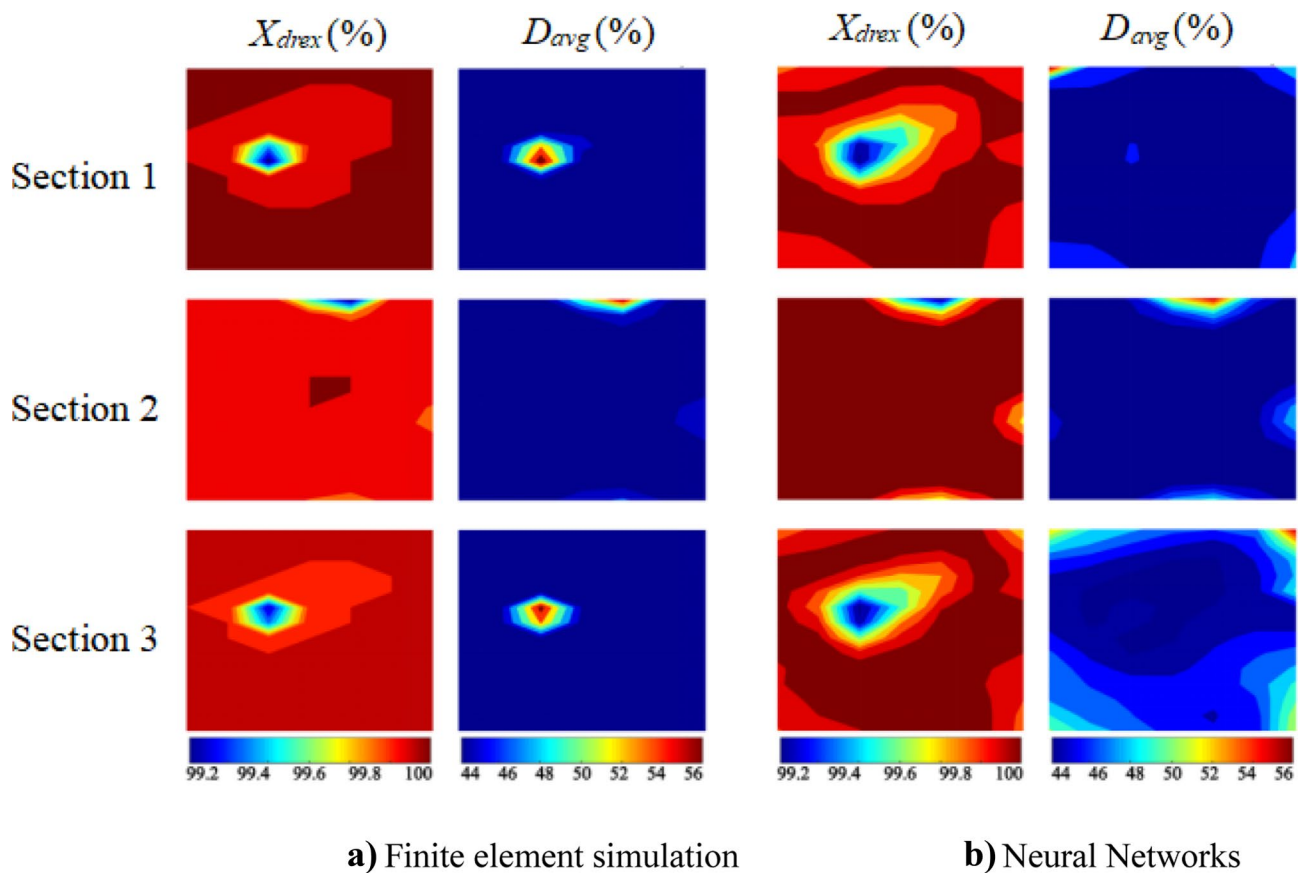


Fig. 14 Comparison of group 3. **a)** Finite element simulation. **b)** Neural networks

5 Conclusions

1. The true stress–strain curve of the thermal deformation of 30Cr2Ni4MoV steel was obtained through a hot compression test, and the constitutive equation of the thermal deformation of the material was constructed. On the basis of the statistics and analysis of the microstructure of the hot compressed sample, the microstructure evolution model of thermal deformation, including the dynamic recrystallization critical condition, dynamic recrystallization volume fraction, and dynamic recrystallization grain size model, was constructed.
2. With the aid of the secondary development interface provided by Deform, the mathematical model was programmed, and the orthogonal method was used to set multiple groups of process conditions. Then, the multi-directional forging deformation of 30Cr2Ni4MoV steel was simulated. The analysis of the orthogonal experiment results reveals the influence law of various factors and may serve as a reference for setting related process conditions.
3. According to the differences in the effects of objects and influence weights of various factors in the finite

element simulation, a neural network prediction model for the multi-directional forging deformation of 30Cr2Ni4MoV steel was established. Compared with the results of the finite element simulation, the neural network prediction results showed a more detailed division of microstructure distribution, and have richer detailed information.

Author contribution Junting Luo contributed to the conception of the study. Jingqi Zhao performed the data analyses and wrote the manuscript. Zheyi Yang made an important contribution to the simulation and data analysis process. Yongbo Jin performed the experiment. Chunxiang Zhang helped perform the analysis with constructive discussions.

Funding This project is supported by the Natural Science Foundation of Hebei Province, China (Grant No. E2019203005).

Availability of data and material The datasets used or analyzed during the current study are available from the authors on reasonable request.

Code availability The raw/processed data required to reproduce these findings cannot be shared at this time as the data also forms part of an ongoing study.

Declarations

Ethics approval The paper is original and has not been published before and is not currently being considered for publication elsewhere.

Consent to participate All the authors listed agree to participate.

Consent for publication All the authors listed agree to publish.

Conflict of interest The authors declare no competing interests.

References

- He JL, Cui ZS, Chen F, Xiao YH, Ruan LQ (2013) The new ductile fracture criterion for 30Cr2Ni4MoV ultra-super-critical rotor steel at elevated temperatures. *Mater Des* 52:547–555
- Chen F, Cui ZS, Sui DS, Fu B (2012) Recrystallization of 30Cr2Ni4MoV ultra-super-critical rotor steel during hot deformation. Part III: metadynamic recrystallization. *Mater Sci Eng, A* 540:46–54
- Chen F, Cui ZS, Chen SJ (2011) Recrystallization of 30Cr2Ni4MoV ultra-super-critical rotor steel during hot deformation. Part I: dynamic recrystallization. *Mater Sci Eng A* 528(15):5073–5080
- Zhang XZ, Liu ZL, Liu JS, Dang SE (2020) Evolution and evaluation of duplex grain of as-cast 30Cr2Ni4MoV steel during heat treatment. *Mater Sci* 26(3):281–286
- Zhou P, Ma QX (2017) Dynamic recrystallization behavior and constitutive modeling of as-Cast 30Cr2Ni4MoV steel based on flow curves. *Met Mater Int* 23(2):359–368
- Zhu QF, Li L, Ban CY, Zhao ZH, Zuo YB, Cui JZ (2014) Structure uniformity and limits of grain refinement of high purity aluminum during multi-directional forging process at room temperature. *Trans Nonferrous Met Soc China* 24(5):1301–1306
- Kavosi J, Saei M, Kazeminezhad M, Dodangeh A (2014) Modeling of dislocation density and strength on rheoforged A356 alloy during multi-directional forging. *Comput Mater Sci* 81:284–289
- Zhang ZX, Qu SJ, Feng AH, Shen J (2017) Achieving grain refinement and enhanced mechanical properties in Ti–6Al–4V alloy produced by multidirectional isothermal forging. *Mater Sci Eng A* 692:127–138
- Miura H, Maruoka T, Yang X, Jonas JJ (2012) Microstructure and mechanical properties of multi-directionally forged Mg–Al–Zn alloy. *Scr Mater* 66(1):49–51
- Gao ZY, Grandhi RV (2000) Microstructure optimization in design of forging processes. *Int J Mach Tool Manuf* 40(5):691–711
- Chamanfar A, Valberg HS, Templin B, Plumeri JE, Misiolek WZ (2000) Development and validation of a finite-element model for isothermal forging of a nickel-base superalloy. *Materialia* 6:100319
- Srinivasan R, Ramnaraya NV, Deshpande U, Jain V, Weiss I (1993) Computer simulation of the forging of fine grain IN-718 alloy. *Metall Trans A* 24(9):2061–2069
- Qian DS, Pan Y (2013) 3D coupled macro–microscopic finite element modelling and simulation for combined blank-forging and rolling process of alloy steel large ring. *Comput Mater Sci* 70:24–36
- He A, Wang XT, Xie GL, Yang XY (2015) Modified Arrhenius-type constitutive model and artificial neural network-based model for constitutive relationship of 316 LN stainless steel during hot deformation. *J Iron Steel Res Int* 22(8):721–729
- Jin YB, Hao X, Yang ZY, Zhang LL, Zhang CX, Wang SR, Luo JT (2019) Constitutive equation of GH4169 superalloy and microstructure evolution simulation of double-open multidirectional forging. *Metals* 9(11):1146
- Fang S, Liu Z, Yi W, Shi Z (2010) Finite element simulation of machining of Ti-6Al-4V alloy with thermodynamical constitutive equation. *Int J Mach Tools Manuf* 49(5–8):431–439
- Park NK, Kim IS, Na YS, Yeom JT (2001) Hot forging of a nickel-base superalloy. *J Mater Process Technol* 111(1–3):98–102
- Kermanpur A, Tin S, Lee PD, Mclean M (2004) Integrated modeling for the manufacture of aerospace discs: grain structure evolution. *JOM* 56(3):72–78
- Guo Q, Yan HG, Chen ZH, Zhang H (2007) Grain refinement in as-cast AZ80 Mg alloy under large strain deformation. *Mater Charact* 58(2):162–167
- Bahmani A, Arthanari S, Shin KS (2000) Improved corrosion resistant and strength of a magnesium alloy using multi-directional forging (MDF). *Int J Mach Tools Manuf* 105(1–4):785–797
- Miura H, Yu G, Yang X (2011) Multi-directional forging of AZ61Mg alloy under decreasing temperature conditions and improvement of its mechanical properties. *Mater Sci Eng A* 528(22–23):6981–6992
- Wu GP, Wang SA, Huang W, Liu TH, Yin Y, Liu YH (2016) Application of BP and RBF neural network in classification prognosis of hepatitis B virus reactivation. *Proc 2016 Int Conf Electr Eng Comput Sci (ICEECS2016)* 54–58
- Sun ZC, Wang XQ, Zhang J, Yang H (2014) Prediction and control of equiaxed α in near- β forging of TA15 Ti-alloy based on BP neural network: for purpose of tri-modal microstructure. *Mater Sci Eng A* 591:18–25

Publisher's note Springer Nature remains neutral with regard to jurisdictional claims in published maps and institutional affiliations.